Weather and Climate Extremes 44 (2024) 100660

Contents lists available at ScienceDirect

Weather and Climate Extremes

journal homepage: www.elsevier.com/locate/wace

The synergistic effect of the preceding winter mid-latitude North Atlantic and summer tropical eastern Indian Ocean SST on summer extreme heat events in northern China

Hao Wang [a], Jianping Li [a,b,*], Fei Zheng [c,d,**], Fei Li [e], Ning Wang [a], Yue Sun [a]

[a] Frontiers Science Center for Deep Ocean Multispheres and Earth System-Key Laboratory of Physical Oceanography-Institute for Advanced Ocean Studies-Academy of the Future Ocean, Ocean University of China, Qingdao, 266100, China
[b] Laoshan Laboratory, Qingdao, 266237, China
[c] School of Atmospheric Sciences, Key Laboratory of Tropical Atmosphere-Ocean System, Ministry of Education, Sun Yat-sen University, Zhuhai, 519082, China
[d] Southern Marine Science and Engineering Guangdong Laboratory, Zhuhai, 519082, China
[e] Jining Meteorological Bureau, Jining, 272000, China

ARTICLE INFO

Keywords:
Extreme heat events
Northern China
Indian ocean
Atlantic
Synergistic effect

ABSTRACT

Summer extreme heat events happen frequently in northern China during recent decades, which have serious impacts on the society and ecosystem. The present study reveals that there is a synergistic effect of the preceding winter positive mid-latitude North Atlantic SST anomaly (pMNA SSTA) and summer negative tropical eastern Indian Ocean SST anomaly (nTEI SSTA) on strengthening the summer extreme heat events in northern China. The extreme heat events are stronger and more frequent when the two factors cooccur, and the probability of a strengthened extreme heat events is higher, which indicates a synergistic effect of the two factors. The preceding winter pMNA SSTA and summer nTEI SSTA exert their synergistic effect through a series of coupled oceanic-land-atmospheric bridges. The preceding winter pMNA SSTA could lead to an anomalous anticyclone over central Asia via the eastward propagating Rossby wave, which decreases snowfall and the subsequent snow cover there. The negative snow cover anomaly may persist into spring and induce a local anomalous anticyclone in spring via the snow-hydrological effect, which decreases the precipitation over the southern flank of the anomalous anticyclone. The decreased soil moisture persists into summer and induces the eastward propagating Rossby wave, and favors the increase of atmosphere thickness over northern China. The summer nTEI SSTA can also induce the anomalous anticyclone over northern China via the northeastward Rossby wave propagation. Thus, the two factors exhibit evident synergistic effect on the atmospheric circulation anomaly over northern China. The anomalous anticyclone corresponds to the increased atmosphere thickness, which favors the increase of air temperature in northern China and strengthening of extreme heat events. Therefore, the preceding winter pMNA SSTA and summer nTEI SSTA have significant synergistic effect on strengthening the summer extreme heat events in northern China.

1. Introduction

Extreme heat events are reported to intensify and occur more frequently under global warming, and the extreme temperatures on land are even projected to increase more and quicker than the global mean temperature (Meehl and Tebaldi 2004; Fischer and Schär 2010; Perkins 2015; IPCC, 2023; Wang and Yan 2021). The occurrence of extreme heat events poses a huge threat to the ecosystem and disrupts normal life of people (e.g. Coumou and Rahmstorf 2012; Horton et al., 2016; Mora et al., 2017). Northern China holds particular importance in the country, serving as a hub for heavy industry and a crucial agricultural region. However, extreme heat events strike this area frequently. For instance,

* Corresponding author. Frontiers Science Center for Deep Ocean Multispheres and Earth System-Key Laboratory of Physical Oceanography-Institute for Advanced Ocean Studies-Academy of the Future Ocean, Ocean University of China, Qingdao, 266100, China.
** Corresponding author. School of Atmospheric Sciences, Key Laboratory of Tropical Atmosphere-Ocean System, Ministry of Education, Sun Yat-sen University, Zhuhai, 519082, China.
E-mail addresses: ljp@ouc.edu.cn (J. Li), zhengf35@mail.sysu.edu.cn (F. Zheng).

https://doi.org/10.1016/j.wace.2024.100660
Received 19 January 2024; Received in revised form 25 February 2024; Accepted 14 March 2024
Available online 15 March 2024

in 2018, a severe heat wave occurred in northern China, with daily maximum temperature reaching up to 39 °C in some provinces, as reported by the China Meteorological Administration (CMA). In 2023, another round of extreme heat events swept through northern China, with many stations reporting maximum daily temperatures exceeding 40 °C. This marks one of the highest temperatures in history, affecting over 200 million people in the region.

Extreme temperature events are linked with anomalous large-scale atmospheric circulation (Grotjahn et al., 2016). The presence of a robust local anomalous anticyclone, often identified as atmospheric blocking, plays an important role in triggering extreme heat events (Parker et al., 2014; Perkins-Kirkpatrick and Gibson, 2017; Deng et al., 2018; Wang et al., 2023a; Xie and Zhou 2023). This anomalous anticyclone is known to reduce cloud cover over the area, facilitating increased incoming solar radiation, thereby favoring a rise in air temperature (Pfahl and Wernli 2012; Black et al., 2004; Gershunov et al., 2009; Chen and Lu 2015; Lu and Chen 2016). Furthermore, the local anomalous anticyclone can elevate air temperature via the thickened atmosphere thickness, thereby promoting the intensification and the frequency of extreme heat events (Li et al., 2020a). Previous studies pointed out that the massive exchanges of mass and energy at high and low latitudes are of importance for the formation and maintenance of atmospheric blocking, which thereby leads to strong changes of weathers (Yao et al., 2024). The atmospheric blocking system could work with other systems and further lead to temperature extremes (Li et al., 2020b). Yang et al. (2021) compared two common types of extreme heat events in northern East Asia and found that the local anomalous anticyclone is responsible for both event types. Notably, the strong extreme heat event in the summer of 2010 in Russia, which caused over 50 000 deaths, was associated with a strong and long-lived regional anticyclonic anomaly (Dole et al., 2011; Schneidereit et al., 2012). Previous studies highlight the crucial role of strong large-scale local anomalous anticyclone as the driver of extreme heat events in northern China (e.g. Gong et al., 2004; Wang et al., 2018; Li et al. 2019; Su and Dong 2019).

From a planetary scale perspective, remote climatic signals can trigger and exacerbate extreme heat events by influencing local atmospheric circulation. The sea surface temperature anomaly (SSTA) is an important remote surface forcing and a useful predictor for extreme heat events (Domeisen et al., 2023). Previous studies have demonstrated that the El Niño-Southern Oscillation (ENSO) has an impact on the extreme heat events in China, especially in southern China. El Niño tends to significantly amplify the frequency, duration and magnitude of heatwaves, while La Niña has the opposite effect (Luo and Lau, 2019; Hong et al., 2023; Wei et al., 2023).

Although ENSO has evident impact on the SST variability in tropical Indian Ocean (Xie et al., 2009, 2010; Chowdary et al., 2012), the Indian Ocean SST exhibits noticeable internal variability that is independent of ENSO (e.g. Han et al., 2014; Zhang et al., 2021). The tropical Indian Ocean SST variations could have impacts on weather and climate globally. Previous studies suggested that summer Indian Ocean SST can influence surface air temperature over Saudi Arabia via teleconnection (Hasanean and Almazroui, 2017; Almazroui and Hasanean 2020). Additionally, some studies pointed out that summer tropical Indian Ocean SST variability has significant impacts on the surface air temperature and extreme heat events in the whole eastern China by emanating the kelvin wave propagation (Hu et al., 2011, 2012). The presence of warm (cold) tropical Indian Ocean SST is favorable for the decrease (increase) in air temperature in northern China by triggering the anomalous atmospheric circulation over northern China (Hu et al., 2011).

In addition to the Indian Ocean, the North Atlantic SST variation can also exert important climatic impacts on remote areas (e.g. Czaja and Frankignoul 1999; Sun et al., 2017; Wang et al., 2023b). Some studies have suggested that winter North Atlantic SSTA can influence the air temperature and precipitation in subsequent seasons in Siberia via triggering the atmospheric teleconnections (e.g. Sun et al., 2015; Chen and Wu 2017; Chen et al., 2021). Liu et al. (2014) pointed out that the mid-latitude North Atlantic (MNA) SSTA can trigger the Eurasian teleconnection, thereby affecting the climate over the Eurasian continent. This Eurasian teleconnection has recently been seen as a potential influencing factor for snowfall over central Eurasian continent in the cold season (Zhang et al., 2023).

Since both of the Indian Ocean and North Atlantic SST variability have potentials to have impacts on the atmospheric circulation and resultant anomalous weather and climate in northern China, whether they have a joint effect on the extreme heat events in northern China and what is the mechanism behind the joint effect are unknown. In this study, we use the joint effect diagnostic method proposed by Li et al. (2019a), and investigate the possible synergistic effect of the Indian Ocean and North Atlantic SSTA. This method has been extensively used in various studies investigating the joint effect of two factors on weather and climate (Sun and Li 2022; Tang et al., 2023), and it is particularly useful while studying the extreme events (Wang et al., 2022, 2023a). For instance, Wang et al. (2022) found that there is a synergistic effect of the preceding winter positive phase of Northern Hemisphere Annular Mode and the spring negative tropical North Atlantic SSTA on weakening the spring extreme cold events in the mid-high latitudes of East Asia. Wang et al. (2023a) investigated the synergistic effect of the summer positive NAO and positive northwest pacific SSTA on extreme heat events in the central–eastern China, and found that the extreme heat events are significantly enhanced by the two factors via a series of atmospheric bridges.

In this paper, we will focus on the possible synergistic effect of the tropical Indian Ocean and North Atlantic SST on the extreme heat events in northern China and try to reveal the mechanism of the synergistic effect. The remainder of the paper is structured as follows: section 2 describes the data and methods used in this study. The characters and mechanisms of the synergistic effect are presented in section 3, and section 4 gives the conclusions of the paper.

2. Data and methods

2.1. Data

The datasets used in the research are listed in Table 1. The Hadley Centre Sea Ice and Sea Surface Temperature dataset version 1 (HadISST1) is employed to provide the observational SST data (Rayner

Table 1
Datasets employed in this study.

Variable	Period of record	Horizontal resolution	Source
SST	1870–3/2023	1° × 1°	HadISST1 (version 1.1) from the Met Office Hadley Center (Rayner et al., 2003)
Extreme temperature indices	1901–2018	1.25° × 1.875°	HadEX3 from the Met Office Hadley Center (Dunn and Coauthors, 2020)
Geopotential height, winds, snow cover, volumetric soil water layer 1, total precipitation, water vapor flux, vertically integrated moisture divergence and surface latent heat flux	1950-4/2023	0.25° × 0.25° (atmosphere) 0.1° × 0.1° (land)	The European Centre for Medium-Range Weather Forecasts (ECMWF) reanalysis version 5 (Hersbach and Coauthors, 2020)
The Global SAT time series	1850–4/2023	/	HadCRUT4 from Met Office Hadley Center (Morice et al., 2012)

et al., 2003). It covers the period 1870−3/2023, and has a horizontal resolution of 1° × 1°. The HadEX3 dataset, which is on a 1.25° × 1.875° grid from 1901 to 2018, contains the temperature extremes indices (Dunn and Coauthors, 2020). We used two temperature extremes indices, TXx (monthly highest value of the daily minimum temperature) and TX90p (the percentage of time when the daily maximum temperature is higher than the 90th percentile). For the atmospheric and land variables, we used the European Centre for Medium-Range Weather Forecasts (ECMWF) reanalysis version 5 (ERA5) dataset for geopotential height, winds, snow cover, soil moisture (represented by the volumetric soil water layer 1 in the dataset), total precipitation, water vapor flux, vertically integrated moisture divergence and surface latent heat flux (Hersbach and Coauthors, 2020). The dataset covers the period 1950−4/2023 on a 0.25° × 0.25° (atmosphere) or 0.1° × 0.1° (land) grid. We also used the global surface temperature time series in the HadCRUT4, which covers the period 1850−4/2023, to remove the global warming signal (Morice et al., 2012).

Owing to the reason that HadEX3 dataset ends at 2018, we constrained our analysis to the period 1961–2018.

2.2. Statistical methods

In this paper, we define winter as December–January−February, spring as March–April−May and summer as June–July−August. For instance, the preceding winter in 2018 is from December 2017 to February 2018. The northern China is defined as the area of 37.5°–50°N, 110°−125°E, which is framed in Fig. S1. The statistical significance test used in this study is the two-tailed Student's *t*-test. We remove the global warming signal from all variables in this study by using the linear regression.

2.3. The combined effect diagnostic method

The combined effect diagnostic method proposed by Li et al. (2019a) is employed in this study to determine the existence of a synergistic effect.

Here, we assume that two factors F_1 and F_2 are studied. Each of them can be divided into positive, neutral and negative phases. Assuming that the positive phases of the two factors are studied, thus they can be represented as F_1^+ and F_2^+. Therefore, three types of events can be defined by the occurrences of F_1^+ and F_2^+. Firstly, joint events $F_1^+ \oplus F_2^+$ denote the cases when F_1^+ and F_2^+ cooccur. Secondly, $F_1^+ \backslash F_2^+$ denotes the cases when F_1^+ occurs without F_2^+, and the cases are termed as single F_1^+ events. Similarly, we can also tell the type of $F_2^+ \backslash F_1^+$, which is termed as single F_2^+ events. By comparing the response T in different events, we can tell the type of combined effect of the two factors F_1^+ and F_2^+. If $|T|$ of $F_1^+ \oplus F_2^+$ is greater than the maximum of $|T|$ of $F_1^+ \backslash F_2^+$ and $F_2^+ \backslash F_1^+$, there will be a synergistic effect. If $|T|$ of $F_1^+ \oplus F_2^+$ is smaller than the minimum of $|T|$ of $F_1^+ \backslash F_2^+$ and $F_2^+ \backslash F_1^+$, there will be an antagonistic effect. However, if $|T|$ of $F_1^+ \oplus F_2^+$ is between $|T|$ of $F_1^+ \backslash F_2^+$ and $F_2^+ \backslash F_1^+$, there will be no evident combined effect. We focus on the synergistic effect in this study, and it can be statistically determined by this method.

Considering the limited occurrence of different types of events, we used the bootstrap resampling method to assess the statistical significance of the synergistic effect (Deser et al., 2017, 2018; Tang et al., 2023; Wang et al. 2023). 1 000 bootstrapped composites are generated based on the 3 types of events. By comparing the difference between joint events and two types of single events, we can determine the statistical significance of the synergistic effect. If the value 0 falls outside (inside) the range between 10th- and 90th-percentile values, the synergistic effect is considered to be significant (insignificant).

2.4. The Rossby wave propagation analysis method

To clearly show Rossby wave propagation, we use the Rossby wave ray tracing theory in a horizontally non-uniform basic flow, and the trajectory of the stationary Rossby wave train can be traced and the pathway of the impacts of two factors can be characterized (Li and Li 2012; Li et al., 2015, 2019b, 2021; Zhao et al., 2015, 2019).

Based on the previous theory, the dispersion relationship of the Rossby wave frequency and wavenumber in a horizontally non-uniform flow can be written as (Karoly 1983; Li and Nathan 1997; Li and Li 2012; Li et al., 2015; Zhao et al., 2015, 2019):

$$\omega = \overline{u}_M k + \overline{v}_M l + \frac{\overline{q}_x l - \overline{q}_y k}{k^2 + l^2}, \tag{1}$$

where ω is the wave frequency; k and l are the zonal and meridional wavenumbers, respectively; $(\overline{u}_M, \overline{v}_M) = (\overline{u}, \overline{v})/\cos\varphi$ is the Mercator projection of zonal and meridional winds; φ is the latitude; $\overline{q} = \nabla_M^2 \overline{\psi}/\cos^2\varphi + f$ is the absolute vorticity of the background; and $\overline{q}_x$ and $\overline{q}_y$ are the zonal and meridional gradients of $\overline{q}$, respectively.

If we let $K = \sqrt{k^2 + l^2}$ indicate the total wavenumber, the zonal and meridional components of the group velocity will take the form as:

$$u_g = \frac{\partial \omega}{\partial k} = \overline{u}_M + \frac{(k^2 - l^2)\overline{q}_y - 2kl\overline{q}_x}{K^4}, \tag{2a}$$

$$v_g = \frac{\partial \omega}{\partial l} = \overline{v}_M + \frac{(k^2 - l^2)\overline{q}_x + 2kl\overline{q}_y}{K^4}. \tag{2b}$$

As the background flow changes along the ray, the wavenumbers determined by the kinematic wave theory can be written as (Whitham 1960):

$$\frac{\mathrm{d}_g k}{\mathrm{d}t} = -\frac{\partial \omega}{\partial x} = -k\frac{\partial \overline{u}_M}{\partial x} - l\frac{\partial \overline{v}_M}{\partial x} - \frac{1}{K^2}\left(l\frac{\partial \overline{q}_x}{\partial x} - k\frac{\partial \overline{q}_y}{\partial x}\right), \tag{3a}$$

$$\frac{\mathrm{d}_g l}{\mathrm{d}t} = -\frac{\partial \omega}{\partial y} = -k\frac{\partial \overline{u}_M}{\partial y} - l\frac{\partial \overline{v}_M}{\partial y} - \frac{1}{K^2}\left(l\frac{\partial \overline{q}_x}{\partial y} - k\frac{\partial \overline{q}_y}{\partial y}\right), \tag{3b}$$

where $\frac{\mathrm{d}_g}{\mathrm{d}t} = \frac{\partial}{\partial t} + \overline{u}_g\frac{\partial}{\partial x} + \overline{v}_g\frac{\partial}{\partial y}$ is the material derivative moving with the group velocity. As can be seen from Equation (3), the zonal and meridional wavenumbers vary along the wave ray, which is different from the original theory proposed by Hoskins and Karoly (1981). Equations (2) and (3) form the wave ray tracing equation set. Thus, the initial local meridional wave number l is determined by Equation (1) once the initial position and zonal wavenumber k are given. Then, the wave ray tracing equation set will be able to obtain the corresponding wave ray trajectory. In the large-scale Rossby wave, the integration is terminated once the local meridional wavelength is less than 1 000 km.

2.5. The perturbation hypsometric equation

The perturbation hypsometric equation is an effective tool to diagnose the influence of the large-scale local anomalous atmospheric circulation on the local air temperature, and the perturbation hypsometric equation takes the form as (Li et al., 2021):

$$\langle T \rangle' = \frac{g_0}{R}\left(\ln\frac{p_1}{p_2}\right)^{-1}\Delta Z', \tag{4}$$

where $\langle T \rangle'$ is the anomaly of the mean temperature of the layer, $\Delta Z'$ is the anomalous atmospheric thickness between two pressure layers p_1 and p_2, g_0 is the gravitational acceleration, and R is the gas constant of dry air. According to Equation (4), the perturbation mean air temperature of the atmospheric layer is proportional to the perturbation atmospheric thickness bounded by isobaric surfaces. Therefore, the anomalous atmospheric thickness could indicate the variability of the mean air temperature of the atmospheric layer.

3. The presence of the synergistic effect of the preceding winter mid-latitude North Atlantic and summer tropical eastern Indian Ocean SST on extreme heat events in northern China

Fig. 1 shows the correlation maps between the summer northern China temperature extremes indices and SST in summer and preceding winter. The MNA SST variability in preceding winter is significantly positively correlated with both summer TXx and TX90p in northern China, indicating that the occurrence of the positive MNA SST anomaly (pMNA SSTA) in preceding winter corresponds to higher daily maximum temperature and more frequent high-temperature days in northern China in summer (Fig. 1a and b). When it comes to summer, there are significant negative correlation coefficients between the temperature extremes indices and SST in the tropical Indian Ocean, especially in the tropical eastern Indian Ocean (TEI, Fig. 1c and d). This phenomenon indicates that negative TEI SST anomaly (nTEI SSTA) is associated with a high likelihood of above-normal air temperature and more frequent hot days in northern China. These results imply that both the preceding winter pMNA SSTA (30°−60°N, 20°−50°W) and summer nTEI SSTA (20°S−20°N, 70°−110°E) are favorable for the strengthened extreme heat events in northern China. Thus, we choose the two factors and further investigate if there is a possible synergetic effect.

After selecting the two factors, we categorize them into three types of events based on their occurrence years, using a threshold of 0.6 standard deviation to include more cased. Table 2 lists the numbers and occurrence years of the three types of events, consisting of 7 joint events pMNA⊕nTEI, 10 single pMNA SSTA events and 7 single nTEI SSTA events.

To compare some basic information in different events, we use bar charts showing the averaged factors strengths and local covariances in Fig. 2. Firstly, we note that the averaged amplitudes of the two factors do not differ significantly between the joint events pMNA⊕nTEI and their corresponding single events (Fig. 2a): the averaged pMNA SSTA is 0.46 (0.47) for joint events pMNA⊕nTEI (single pMNA SSTA events), and the averaged nTEI SSTA is −0.19 (−0.21). This result means that there are not significant changes in the strengths of the two factors. Thus, stronger factors leading to stronger responses is not the way of the synergistic effect here.

We also calculate the local covariances between the factors and extreme heat events indices to compare the averaged contribution of different events to the correlation coefficient (Fig. 2b and c). The local covariances between the preceding winter MNA SSTA and TXx (TX90p) are 0.45 (2.52) and 0.10 (0.37) in joint events pMNA⊕nTEI and single pMNA SSTA events, respectively. With regard to the summer TEI SSTA, the local covariances are −0.18 (−0.07) and −0.95 (−0.34) for TXx (TX90p) in joint events pMNA⊕nTEI and single nMNA SSTA events, respectively. The local covariance for preceding winter pMNA SSTA (summer nTEI SSTA) could be up to more than fourfold (twofold) greater in joint events pMNA⊕nTEI than that in its single events. The local covariances are also significant in joint events pMNA⊕nTEI, while they are insignificant in single events for both factors. The larger and significant local covariances between the factors and extreme heat events indices in the joint events imply that there is an amplifying effect of the influences of the factors on the extreme heat events in northern China, which also marks a synergistic effect between the two factors on summer extreme heat events in northern China.

Table 2
Numbers and years of the joint events of preceding winter pMNA and summer nTEI SSTA (pMNA ⊕ nTEI), single preceding winter pMNA SSTA events and single summer nTEI SSTA events.

	Joint events pMNA ⊕ nTEI	Single preceding winter pMNA SSTA events	Single summer nTEI SSTA events
Numbers	7	10	7
Years	1963, 1965, 1968, 1997, 2000, 2004, 2018	1967, 1982, 1996, 1999, 2002, 2005, 2006, 2008, 2009, 2011	1961, 1966, 1978, 1981, 1994, 2013, 2017

Fig. 3 further shows the time series of summer temperature extremes indices in northern China, and the 3 types of events are marked on the plots. It is clear that the amplitudes of two different temperature extreme indices of joint events pMNA⊕nTEI are larger than those of the two types of single events. For the entire time series, the top two largest anomalies for TX90p are associated with joint events pMNA⊕nTEI (Fig. 3c). As for all the selected events, there are 2 joint events pMNA⊕nTEI among the top 3 TXx anomalies years (Fig. 3a). These results highlight the presence of a synergistic effect of the preceding winter pMNA SSTA and summer nTEI SSTA. Based on the bootstrapping method, the synergistic effect of the two factors on the extreme heat events in northern China is statistically significant (Fig. 3b and d). This reinforces the notion that the co-occurrence of preceding winter pMNA SSTA and summer nTEI SSTA amplifies the intensity of extreme heat events in northern China.

To clearly show the difference between the 3 types of events, we plot scatter diagrams illustrating the synergistic effect for the two temperature extreme indices in Fig. 4. The mean temperature indices anomalies of the joint events pMNA⊕nTEI are much higher than those of the single events, with differences exceeding fivefold. It is also worth noting that the same-sign rates for both indices are higher in the joint events pMNA⊕nTEI, indicating that there is a higher probability of strong summer extreme heat events in northern China when the two factors

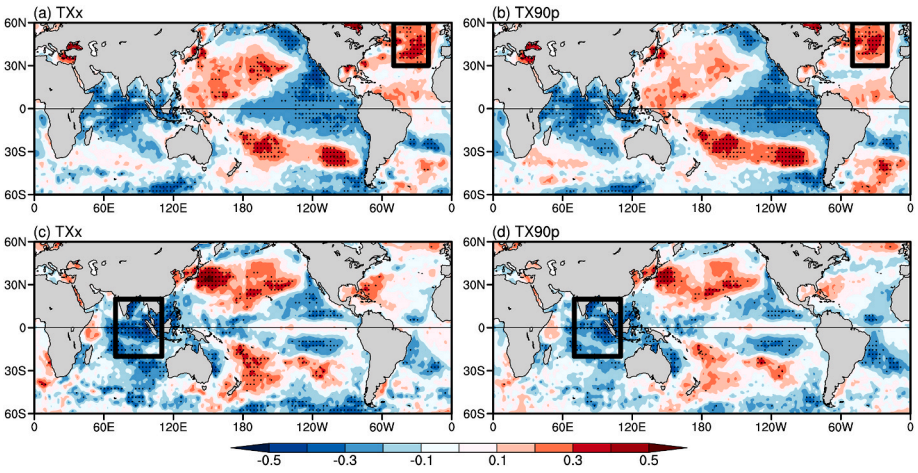

Fig. 1. Correlation maps between the summer northern China extreme temperature indices and (a)–(b) preceding winter and (c)–(d) summer SST. (a) and (c) TXx. (b) and (d) TX90p. Dotted areas indicate significant values at the 95% confidence level based on the Student *t*-test.

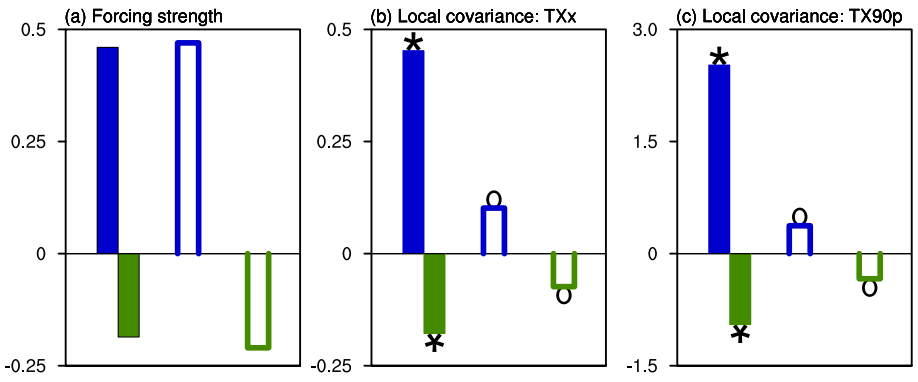

Fig. 2. (a) Composite values of the anomalies of factor strengths in different events. (b) Local covariance between TXx and factors. (c) Local covariance between TX90p and factors. The solid (hollow) blue bars represent preceding winter pMNA SSTA in joint events pMNA⊕nTEI (single preceding winter pMNA SSTA events), and solid (hollow) green bars represent summer nTEI SSTA in joint events pMNA⊕nTEI (single summer nTEI SSTA events). The symbols "*" and "o" represent that the values are significant and insignificant at the 95% confidence level, respectively. (For interpretation of the references to color in this figure legend, the reader is referred to the Web version of this article.)

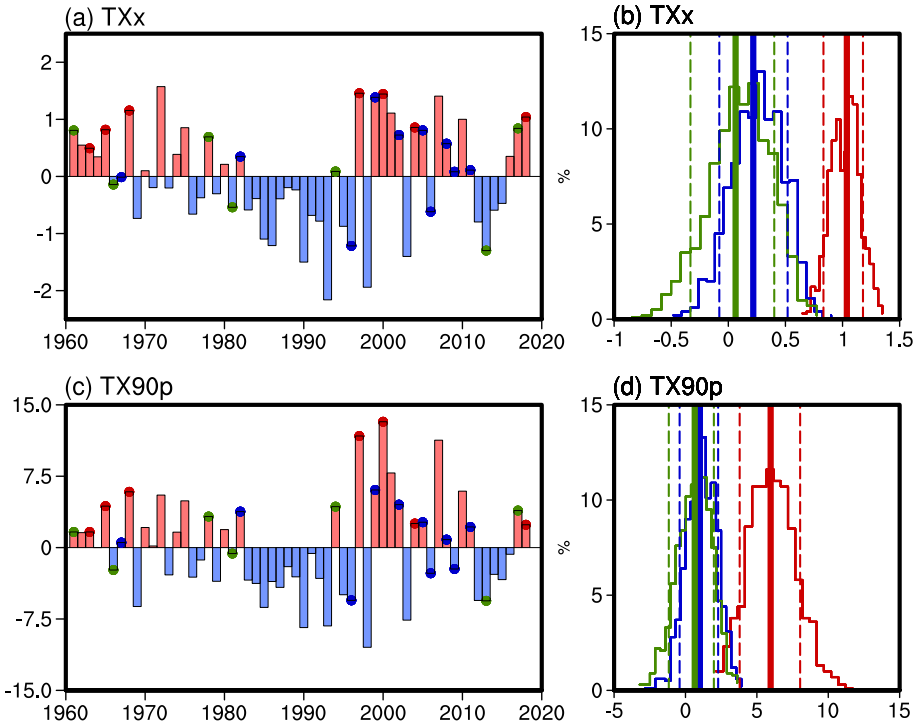

Fig. 3. (a) Time series of the summer area-averaged TXx anomaly (°C) in northern China. The red, blue and green dots represent the joint events of preceding winter pMNA SSTA and summer nTEI SSTA (pMNA⊕nTEI), single preceding winter pMNA SSTA events and single summer nTEI SSTA events respectively. (b) Probability distribution of the summer area-averaged TXx anomaly in northern China. The dashed vertical lines represent the 10th and 90th percentile of the 1 000 bootstrapped anomalous TXx values in different events. (c) As in (a), but for TX90p anomaly (%). (d) As in (b), but for TX90p anomaly. (For interpretation of the references to color in this figure legend, the reader is referred to the Web version of this article.)

cooccur, which also highlights the synergistic effect of the preceding winter pMNA SSTA and summer nTEI SSTA. Both of the larger amplitudes of the extreme heat events indices and same-sign rates highlight that there is a significant synergistic effect of the preceding winter pMNA SSTA and summer nTEI SSTA on strengthening the extreme heat events in northern China, and people in northern China is likely to experience a scorching summer when the two factors cooccur.

To show the spatial distribution of the extreme heat events anomaly, we plot the composite maps of summer temperature extremes index anomalies for different events in Fig. 5. In joint events pMNA⊕nTEI, there are significant positive anomalies of extreme heat events in northern China, with the positive anomaly center situated along the coastal area of the Bohai Sea (Fig. 5a and d). However, in the two types of single events, the significant anomaly is absent around northern China. The two factors exhibit a significant synergistic effect on the positive extreme heat event anomaly in northern China, which implies that there are stronger and more frequent summer extreme heat events in northern China when the two factors cooccur.

In Fig. 6, the spatial pattern of same-sign rates of temperature extreme index anomalies in different events is presented. It is evident that the location of the high same-sign rate center aligns with that of the positive temperature extreme index anomalies in the joint events pMNA⊕nTEI (Fig. 6a and b). However, in the two types of single events, the same-sign rate is around, or even less than 50% around northern China. This suggests that there is considerable uncertainty in the variability of the strength and frequency of the extreme heat events if only

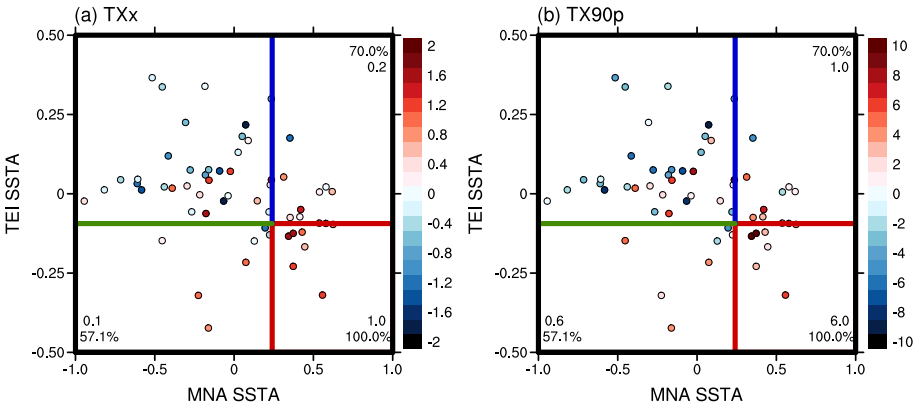

Fig. 4. The scatter diagrams of the synergistic effect. (a) TXx. (b) TX90p. The colors of the dots represent the extreme temperature index anomalies. The lines represent the thresholds of the two factors. (For interpretation of the references to color in this figure legend, the reader is referred to the Web version of this article.)

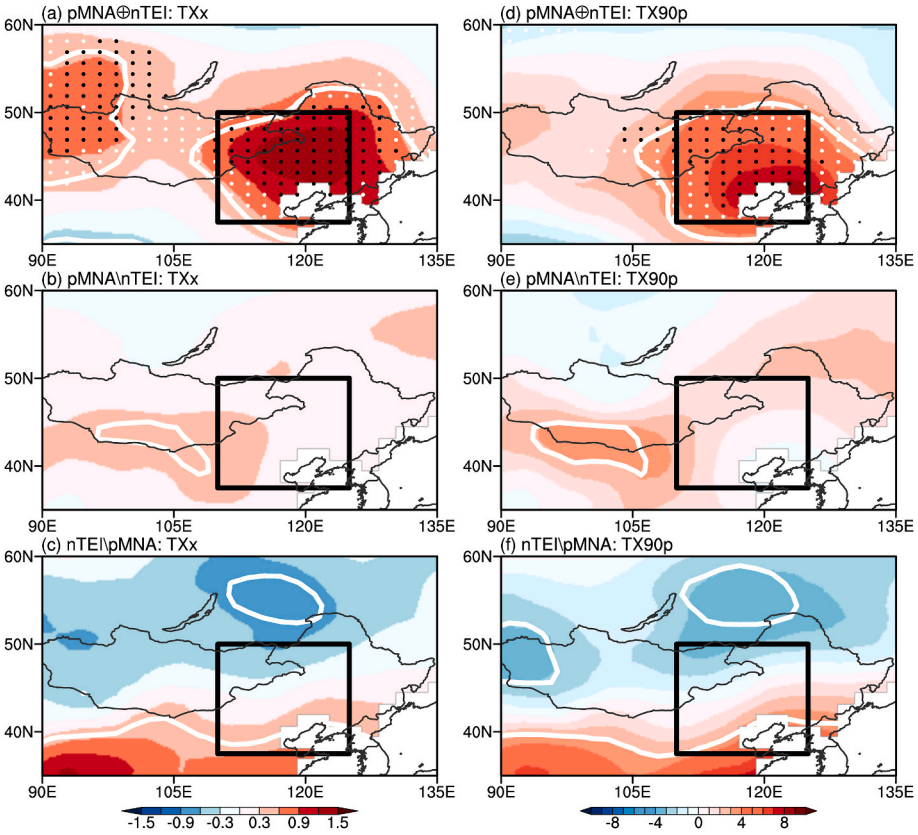

Fig. 5. Composite maps of summer extreme temperature index anomalies for different events. (a) TXx (°C) for the joint events of preceding winter pMNA SSTA and summer nTEI SSTA (pMNA⊕nTEI). The dotted areas indicate the synergistic effect of preceding winter pMNA SSTA and summer nTEI SSTA, and the black dotted areas indicate the synergistic effect is significant at the 90% confidence level based on the bootstrap resampling method. The white contour lines indicate significant values at the 95% confidence level based on the Student *t*-test. (b) As in (a) but for TX90p (%). (c) As in (a), but for the single preceding winter pMNA SSTA events. (d) As in (b), but for the single preceding winter pMNA SSTA events. (e) As in (a), but for the single summer nTEI SSTA events. (f) As in (b), but for the single summer nTEI SSTA events.

one of the factors occurs, highlighting the importance of the synergistic effect when both factors co-occur.

4. The mechanism of the synergistic effect of the preceding winter mid-latitude North Atlantic and summer tropical eastern Indian Ocean SST on extreme heat events in northern China

Fig. 7 presents composite maps of summer 500-hPa geopotential height and 850-hPa wind anomalies in different events, providing insight into the diverse responses of extreme heat events associated with distinct anomalous local atmospheric circulation patterns. In the joint events pMNA⊕nTEI, an anomalous anticyclone is observed over northern China (Fig. 7a), corresponding to significant increase in atmosphere thickness (Fig. 7d). The synergy between the two factors has a pronounced effect on the development of a robust anomalous anticyclone and the substantial thickening of the atmosphere. Additionally, anomalous low-level southerlies over North China Plain bring warmer air from the south, hindering the southward movement of cold air originating from the northern area, thereby favoring the strengthened extreme heat events in northern China (Fig. 7a). The significantly

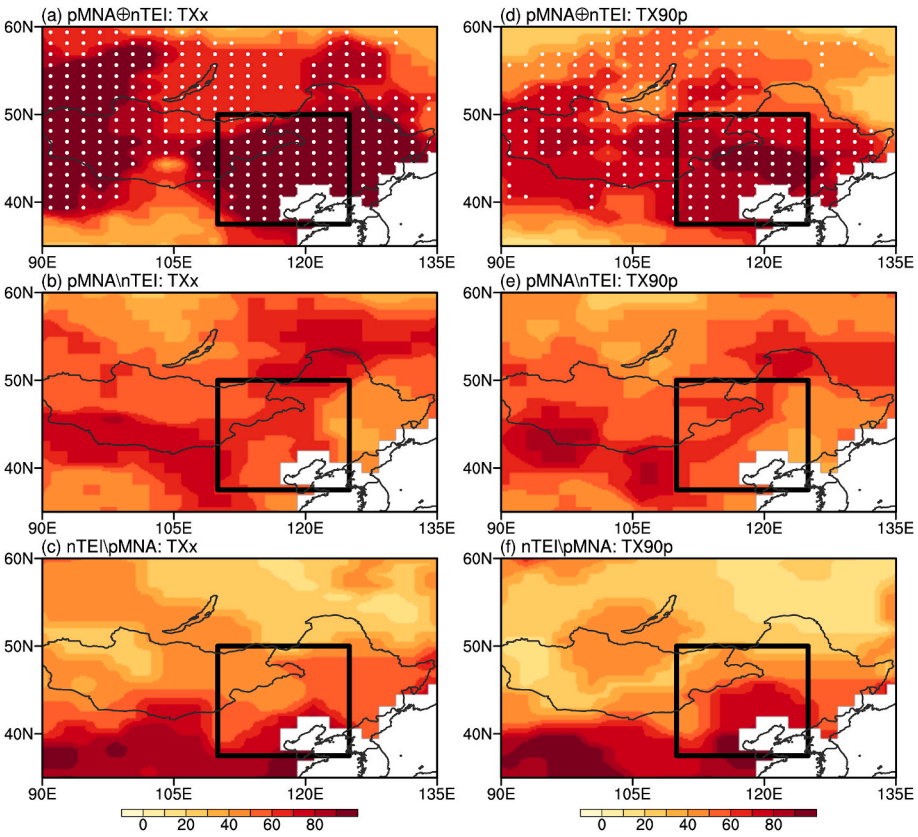

Fig. 6. Same-sign rate (%) maps of extreme index anomalies for different events. (a) TXx for the joint events of preceding winter pMNA SSTA and summer nTEI SSTA (pMNA⊕nTEI). The dotted areas indicate the same-sign rate is higher in the joint events pMNA⊕nTEI than those in the single events. (b) As in (a) but for TX90p. (c) As in (a), but for the single preceding winter pMNA SSTA events. (d) As in (b), but for the single preceding winter pMNA SSTA events. (e) As in (a), but for the single summer nTEI SSTA events. (f) As in (b), but for the single summer nTEI SSTA events.

thickened atmosphere thickness leads to the increase of air temperature of the atmospheric layer, thus favors the strengthening of the extreme heat events (Li et al., 2021).

In the single nTEI SSTA events, an anomalous anticyclone and significantly increased atmosphere thickness are observed over eastern China; however, its location is more southward compared to the anomalous anticyclone in the joint events pMNA⊕nTEI (Fig. 7c and f). Consequently, there is no significant increase in air temperature in the study area, and the strength and frequency of extreme heat events are not significantly influenced in northern China.

In the single pMNA SSTA events, there is not significant atmospheric circulation anomaly over most part of China (Fig. 7b and e). The stronger anomalous atmospheric circulation in joint events pMNA⊕nTEI can also be reflected by the area-averaged values (Fig. S2). Based on the different anomalous atmospheric circulation patterns in different events, we may see that the two factors have significant synergistic effect on generating the strong anomalous anticyclone and increasing the atmosphere thickness over northern China, so the extreme heat events there are significantly strengthened by the heating effect of the thickened atmosphere thickness.

To understand how the two remote factors impact atmospheric circulation over northern China, we explore the potential role of a snow cover bridge. Numerous studies suggested that the snow cover is an essential bridge linking signals in cold seasons to weather and climate in warm seasons (Cohen and Rind 1991; Matsumura et al., 2010; Matsumura and Yamazaki 2012; Xu and Dirmeyer 2013; Tang et al., 2014). In this context, we firstly examine whether there is a possible snow cover bridge before summer. Fig. 8 shows the correlation maps between summer temperature extremes indices in northern China and spring snow cover. Notably, the snow cover in the central Eurasian continent is significantly correlated with the summer extreme heat events in northern China (Fig. 8a and b), which indicates that the decrease of spring snow cover in central Asia (CA) favors the strengthened summer extreme heat events in northern China. Therefore, we focus on the snow cover in CA (40°–60°N, 65°–85°E) and investigate its possible role in transmitting the signal from preceding winter pMNA SSTA to summer atmospheric circulation over northern China.

Fig. 8c and d exhibit the correlation maps between the preceding winter MNA SSTA and summer 500−1 000 hPa atmospheric thickness. The preceding MNA SSTA is significantly positively correlated with the summer atmospheric circulation over northern China, which implies that the preceding pMNA SSTA has the potential to induce an anomalous anticyclone and increase the atmosphere thickness over northern China (Fig. 8c). Nevertheless, the significant relationship between the preceding winter pMNA SSTA and summer anomalous anticyclone disappears after removing the signal of the spring snow cover in CA (Fig. 8d). This result implies that the snow cover is an irreplaceable bridge passing the signal of the preceding winter pMNA SSTA to summer atmospheric circulation over northern China.

The snow-hydrological effect is the way for snow cover to have a delayed impact on the atmosphere, and it can be summarized as: positive (negative) snow cover anomaly could enhance (diminish) soil moisture which persists into following seasons, and further contribute to the cooling (heating) of the atmosphere via latent heat anomaly, and finally trigger a local anomalous cyclone (anticyclone) with decreased (increased) atmosphere thickness (Cohen and Rind 1991; Matsumura et al., 2010; Matsumura and Yamazaki 2012; Xu and Dirmeyer 2013).

As is shown in Fig. 9a, the pMNA SSTA could decrease the central Asian snow cover in the preceding winter, leading to a negative snow cover anomaly by the end of winter, and the snow cover anomaly in CA

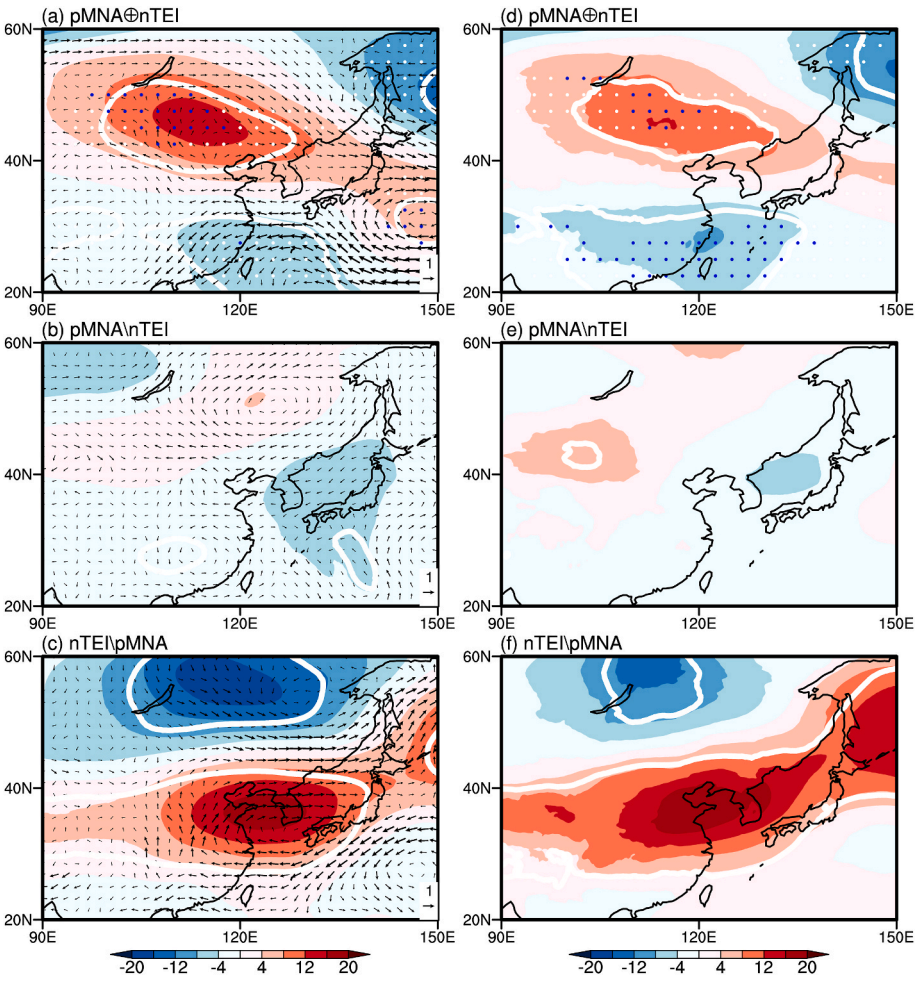

Fig. 7. Composite maps of the summer 500 hPa geopotential height (gpm; shaded) and 850 hPa wind (m s^{-1}; vectors) anomalies in the East Asia for (a) the joint events of preceding winter pMNA SSTA and summer nTEI SSTA (pMNA⊕nTEI), (b) single preceding winter pMNA SSTA events and (c) single summer nTEI SSTA events. (d), (e), (f) As in (a), (b), (c), but for the summer 500−1 000 hPa atm thickness anomalies. The white dotted areas in (a) and (d) indicate the synergistic effect of the preceding winter pMNA SSTA and summer nTEI SSTA, and the blue dotted areas indicate the synergistic effect is significant at the 90% confidence level based on the bootstrap resampling method. The white contour lines indicate significant values at the 95% confidence level based on the Student *t*-test. (For interpretation of the references to color in this figure legend, the reader is referred to the Web version of this article.)

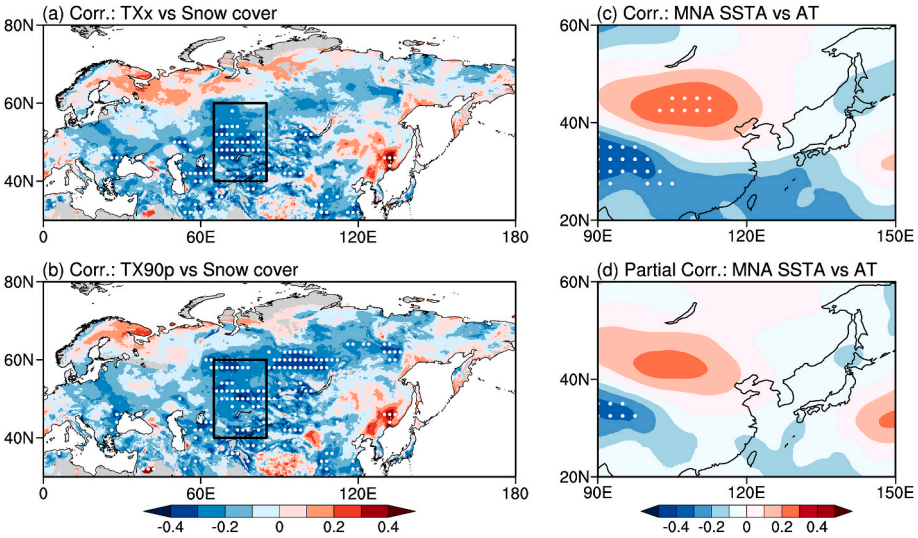

Fig. 8. (a) Correlation maps between TXx and spring snow cover. (b) As in (a), but for TX90p. Correlation maps between the preceding winter MNA SSTA and summer 500−1 000 hPa atmospheric thickness. (c) Original correlation. (d) Partial correlation after removing the spring snow cover in CA. Dotted areas indicate significant values at the 95% confidence level based on the Student *t*-test.

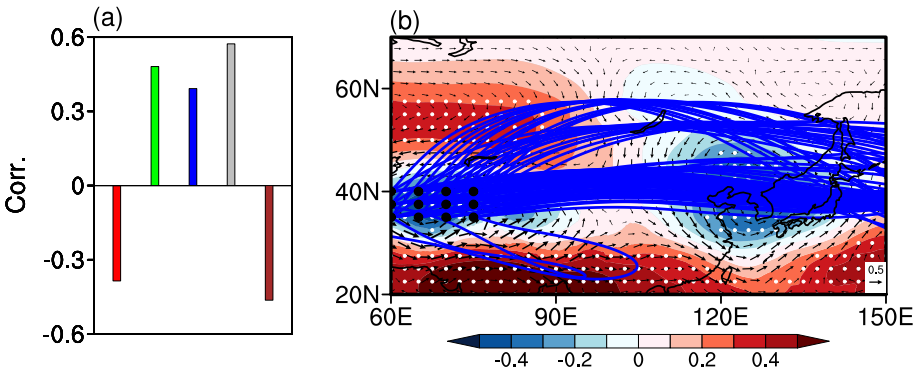

Fig. 9. (a) The correlation coefficients bar chart. The red, green, blue, grey and brown bars represent the correlation coefficients between the preceding winter MNA SSTA and snow cover in CA, the preceding winter and spring snow cover in CA, the spring snow cover in CA and precipitation in SFCA, the spring and summer soil moisture in SFCA, as well as the summer soil moisture and surface latent heat flux in SFCA. (b) Stationary Rossby wave trajectories in the horizontally nonuniform flow (blue curves) with zonal wavenumber $k = 3$, 4 and 5 for pMNA SSTA events in summer at 500 hPa. The shaded areas indicate the correlation map between the summer soil moisture in SFCA and the summer 500 hPa geopotential height. The white dotted areas indicate significant values at the 95% confidence level based on the Student *t*-test. The Rossby wave ray tracing is calculated by adopting the approach by Li and Li (2012), Li et al. (2015, 2019b, 2021) and Zhao et al. (2015). (For interpretation of the references to color in this figure legend, the reader is referred to the Web version of this article.)

would persist into spring. The decreased snow cover in spring could influence the local atmospheric circulation and lead to an anomalous anticyclone over CA via the snow-hydrological effect. There are easterlies over the south flank over the study area in CA (Fig. S3), which further decrease the eastward transport of the water vapor and lead to the moisture divergence (Fig. S4). Thus, the total precipitation decreases on the south flank of central Asia (SFCA, 35°–40°N, 60°–75°E, the black box in Fig. S4), decreasing the soil moisture there. The decreased soil moisture in spring has signal memory, and may persist into summer, which further induces eastward propagating Rossby wave from SFCA, and leads to the anomalous anticyclone with increased atmosphere thickness over northern China (Fig. 9b). Thus, the preceding winter pMNA SSTA could increase the atmosphere thickness in summer over northern China via the snow cover and soil bridges.

How does the pMNA SSTA decrease the snow cover in CA? It is found that the pMNA SSTA could trigger eastward propagating Rossby wave from the Atlantic in the preceding winter, and lead to an anomalous anticyclone over CA (Fig. 10a). The anomalous anticyclone there would decrease the snowfall and lead to the negative snow cover anomaly. It is also worth noting that the summer TEI SSTA has a noticeable impact on the atmospheric circulation over northern China. The occurrence of nTEI SSTA can lead to an anomalous anticyclone over northern China via the northeastward propagating Rossby wave (Fig. 10b). Therefore, the two factors synergistically influence the atmospheric circulation over northern China, leading to a strong anomalous anticyclone and strongly increased atmosphere thickness, and finally have a synergistic effect on strengthening the extreme heat events in northern China.

5. Summary and discussion

The present study shows that there is a synergistic effect of the preceding winter pMNA SSTA and summer nTEI SSTA on strengthening the summer extreme heat events in northern China. The co-occurrence of these two factors is associated with a significantly higher frequency and intensity of extreme heat events, which implies an increased likelihood of a scorching summer in northern China. We also note that the same-sign rate in the joint events pMNA⊕nTEI is higher than those in the two types of single events, which further highlights the existence of the synergistic effect. Although the temperature extremes anomaly of the joint events pMNA⊕nTEI is significantly greater, the strengths of the preceding winter pMNA SSTA and summer nTEI SSTA in the joint events pMNA⊕nTEI are not significantly different from those in their corresponding single events, which indicates that the synergistic effect is not originated from the stronger factors' strength in the joint events pMNA⊕nTEI.

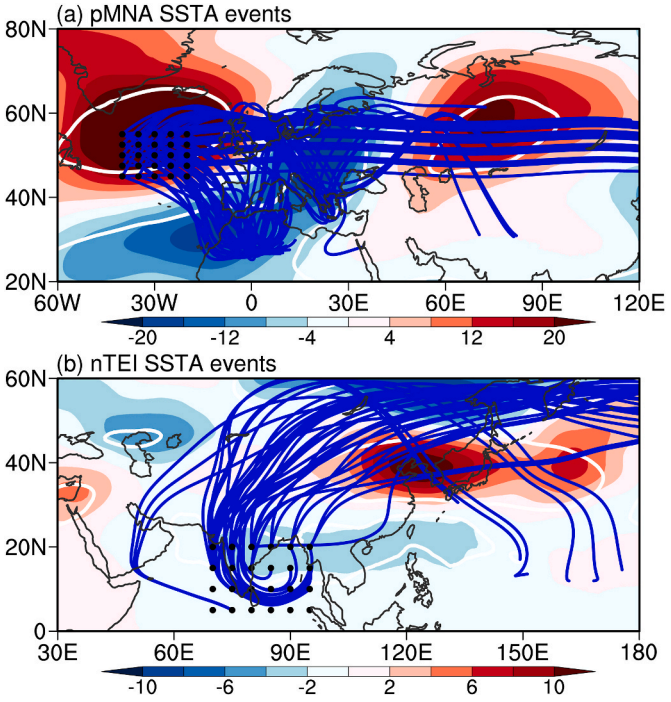

Fig. 10. Stationary Rossby wave trajectories in the horizontally nonuniform flow (blue curves) with zonal wavenumber $k = 3$, 4 and 5 for (a) pMNA SSTA events in preceding winter and (b) nTEI SSTA events in summer at 500 hPa. The shaded areas indicate the composite 500 hPa geopotential height anomalies. The white contour lines indicate significant values at the 90% confidence level based on the Student *t*-test. The Rossby wave ray tracing is calculated by adopting the approach by Li and Li (2012), Li et al. (2015, 2019b, 2021) and Zhao et al. (2015). (For interpretation of the references to color in this figure legend, the reader is referred to the Web version of this article.)

Fig. 11 shows the schematic diagram of the synergistic effect. We show that the two factors exert their synergistic effect via a series of coupled oceanic-land-atmospheric bridges. The preceding winter pMNA SSTA could induce eastward propagating Rossby wave from the North Atlantic, which leads to an anomalous anticyclone over CA. The anomalous anticyclone is unfavorable for the snowfall and results to the diminished snow cover there. The negative snow cover anomaly can

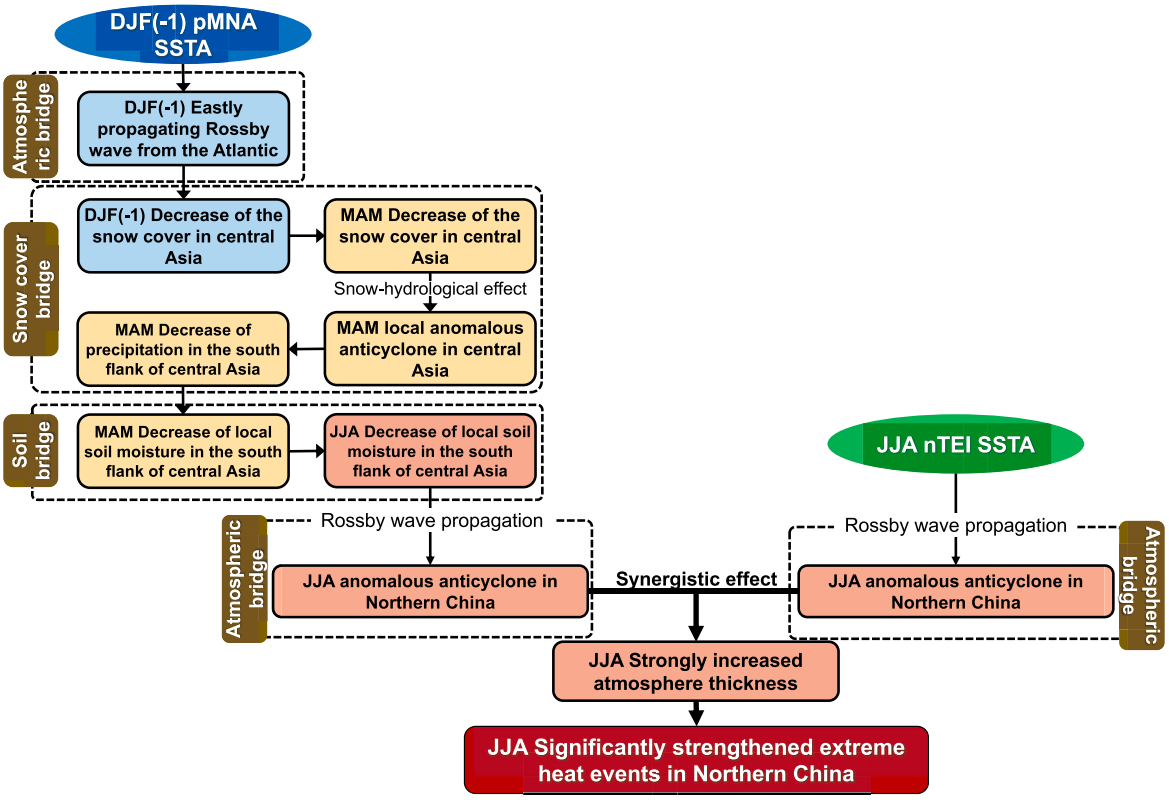

Fig. 11. The schematic diagram illustrating the synergistic effect of the preceding winter pMNA SSTA and summer nTEI SSTA on the summer extreme heat events in northern China.

persist into the subsequent spring, and form a local anomalous anticyclone over CA in spring via the snow-hydrological effect (Cohen and Rind 1991; Matsumura et al., 2010; Matsumura and Yamazaki 2012; Xu and Dirmeyer 2013). The moisture divergence and decreased water vapor transport could decrease the precipitation in SFCA. The decreased soil moisture there has signal memory and may persist into summer, exciting eastward propagating Rossby wave, which corresponds to an anomalous anticyclone and increased atmospheric thickness over northern China. The summer nTEI SSTA is also able to induce an anomalous anticyclone and increase the atmosphere thickness over northern China via inducing the northeastward Rossby wave propagation in summer. Therefore, the two factors act synergistically on increasing the atmosphere thickness over northern China. There is a strong anomalous anticyclone and greatly increased atmosphere thickness over northern China in the joint events pMNA⊕nTEI, on which the two factors show significant synergistic effect. The positive atmospheric thickness can increase the air temperature and favors the strengthened extreme heat events in northern China. From the spatial pattern of the temperature extremes indices anomaly, the center of extreme heat events anomaly lies on the coastal area of the Bohai Sea, and expands outwards. The spatial pattern of the same-sign rate of joint events pMNA⊕nTEI is similar to that of the temperature extremes indices anomaly, which clearly shows that the same-sign rate is much higher in northern China. This result indicates that the probability of the occurrence of strengthened summer extreme heat events is higher for the cooccurrence of the two factors, which highlights the synergistic effect of the preceding winter pMNA SSTA and summer nTEI SSTA. We also used the NCEP–NCAR reanalysis 1 dataset to conduct the analysis (Kalnay et al., 1996), and the results are similar (Figures not shown), which highlights that the synergistic effect is relatively robust.

It is essential to emphasize that our examination focused solely on the synergistic effect of the preceding winter pMNA SSTA and summer nTEI SSTA. Given that synergistic effects may arise from various factors or combinations of factors, it is crucial to explore synergistic effects of other variables. Other regions exhibiting significant correlations with summer extreme heat events in northern China, for instance, the preceding winter southeastern Pacific SST, may also possess the potential to influence extreme heat events in northern China and could contribute to synergistic effects when they coincide with other factors, which is worthy of detailed studies in the future. However, the investigation of the synergistic effect of multiple factors requires longer data periods to accumulate a more extensive set of joint events.

Besides, it is known that ENSO may have prominent impacts on weather and climate in China, and it could interact with the two selected factors. Therefore, we compare the strengths of ENSO in joint events pMNA⊕nTEI and two types of single events in Fig. S5. It can be seen from Fig. S5b that the strength of ENSO in the preceding winter in joint events pMNA⊕nTEI is between those in the two types of single events, which implies that ENSO in the preceding winter may not be related with the amplified summer extreme heat events in joint events pMNA⊕nTEI. As for the Niño 3.4 index in summer, although the amplitude of Niño 3.4 index is stronger in joint events pMNA⊕nTEI, the difference of Niño 3.4 index between the joint events pMNA⊕nTEI and single pMNA SSTA events is not significant based on the bootstrap resampling method. Besides, the same-sign rate of Niño 3.4 index in summer is 71.4% (Fig. S5c), indicating that there is a little uncertainty in the phase of summer Niño 3.4 index when the pMNA and nTEI SSTA cooccur. Whereas, it is still interesting to see a possible but not very robust exacerbating effect on summer Niño 3.4 index by the pMNA and nTEI SSTA, and this phenomenon is worthy of further detailed research in the future. We also removed the ENSO signal from the extreme temperature indices to see if ENSO has an impact on the synergistic effect. As is shown in Fig. S6, although compared with the original time series, there is a slight diminution of the averaged extreme heat indices after removing the preceding winter ENSO, the synergistic effect of the two factors is evident and significant. And the similar results could also

be found after removing the summer Niño 3.4 index anomaly (Fig. S7). The results highlight the stable and robustness of the synergistic effect of the preceding winter mid-latitude North Atlantic and summer tropical eastern Indian Ocean SST on summer extreme heat events in northern China.

CRediT authorship contribution statement

Hao Wang: Writing – review & editing, Writing – original draft, Software, Methodology, Formal analysis, Data curation, Conceptualization. **Jianping Li:** Writing – review & editing, Supervision, Project administration, Funding acquisition, Conceptualization. **Fei Zheng:** Writing – review & editing, Supervision, Formal analysis, Conceptualization. **Fei Li:** Writing – review & editing, Software. **Ning Wang:** Writing – review & editing. **Yue Sun:** Writing – review & editing.

Declaration of competing interest

The authors declare that they have no known competing financial interests or personal relationships that could have appeared to influence the work reported in this paper.

Data availability

Data will be made available on request.

Acknowledgement

We are thankful to all the data providers and two anonymous reviewers. This work is supported by the National Natural Science Foundation of China (NSFC) Project (42288101, 42130607), Laoshan Laboratory (No.LSKJ202202600), and Shandong Natural Science Foundation Project (ZR2019ZD12). We also wish to thank the Center for High Performance Computing and System Simulation, Pilot National Laboratory for Marine Science and Technology (Qingdao) for providing computing resource.

Appendix A. Supplementary data

Supplementary data to this article can be found online at https://doi.org/10.1016/j.wace.2024.100660.

References

Almazroui, M., Hasanean, H.M., 2020. Saudi Arabia's summer surface air temperature and its association with circulation patterns. Int. J. Climatol. 40, 5727–5743. https://doi.org/10.1002/joc.6547.

Black, E., Blackburn, M., Harrison, G., Hoskins, B., Methven, J., 2004. Factors contributing to the summer 2003 European heatwave. Weather 59, 217–223. https://doi.org/10.1256/wea.74.04.

Chen, R., Lu, R., 2015. Comparisons of the circulation anomalies associated with extreme heat in different regions of eastern China. J. Clim. 28, 5830–5844. https://doi.org/10.1175/JCLI-D-14-00818.1.

Chen, S., Wu, R., 2017. Interdecadal changes in the relationship between interannual variations of spring North Atlantic SST and eurasian surface air temperature. J. Clim. 30, 3771–3787. https://doi.org/10.1175/JCLI-D-16-0477.1.

Chen, Y., Luo, D., Zhong, L., Yao, Y., 2021. Effects of barents–kara seas ice and North Atlantic tripole patterns on siberian cold anomalies. Weather Clim. Extrem. 34, 100385 https://doi.org/10.1016/j.wace.2021.100385.

Chowdary, J.S., Xie, S.-P., Tokinaga, H., Okumura, Y.M., Kubota, H., Johnson, N., Zheng, X.-T., 2012. Interdecadal variations in ENSO teleconnection to the indo–western pacific for 1870–2007. J. Clim. 25, 1722–1744. https://doi.org/10.1175/JCLI-D-11-00070.1.

Cohen, J., Rind, D., 1991. The effect of snow cover on the climate. J. Clim. 4, 689–706. https://doi.org/10.1175/1520-0442(1991)004<0689:TEOSCO>2.0.CO;2.

Coumou, D., Rahmstorf, S., 2012. A decade of weather extremes. Nat. Clim. Change 2, 491–496. https://doi.org/10.1038/nclimate1452.

Czaja, A., Frankignoul, C., 1999. Influence of the North Atlantic SST on the atmospheric circulation. Geophys. Res. Lett. 26, 2969–2972. https://doi.org/10.1029/1999GL900613.

Deng, K., Yang, S., Ting, M., Lin, A., Wang, Z., 2018. An intensified mode of variability modulating the summer heat waves in eastern Europe and northern China. Geophys. Res. Lett. 45 (11), 311–361. https://doi.org/10.1029/2018GL079836, 369.

Deser, C., Simpson, I.R., McKinnon, K.A., Phillips, A.S., 2017. The northern Hemisphere extratropical atmospheric circulation response to ENSO: how well do we know it and how do we evaluate models accordingly? J. Clim. 30, 5059–5082. https://doi.org/10.1175/JCLI-D-16-0844.1.

Deser, C., Simpson, I.R., Phillips, Adam.S., McKinnon, K.A., 2018. How well do we know ENSO's climate impacts over North America, and how do we evaluate models accordingly? J. Clim. 31, 4991–5014. https://doi.org/10.1175/JCLI-D-17-0783.1.

Dole, R., Hoerling, M., Perlwitz, J., Eischeid, J., Pegion, P., Zhang, T., Quan, X.-W., Xu, T., Murray, D., 2011. Was there a basis for anticipating the 2010 Russian heat wave? Geophys. Res. Lett. 38 https://doi.org/10.1029/2010GL046582.

Domeisen, D.I.V., Eltahir, E.A.B., Fischer, E.M., Knutti, R., Perkins-Kirkpatrick, S.E., Schär, C., Seneviratne, S.I., Weisheimer, A., Wernli, H., 2023. Prediction and projection of heatwaves. Nat. Rev. Earth Environ. 4, 36–50. https://doi.org/10.1038/s43017-022-00371-z.

Dunn, R.J.H., Coauthors, 2020. Development of an updated global land in situ-based data set of temperature and precipitation extremes: HadEX3. J. Geophys. Res. Atmos. 125, e2019JD032263 https://doi.org/10.1029/2019JD032263.

Fischer, E.M., Schär, C., 2010. Consistent geographical patterns of changes in high-impact European heatwaves. Nat. Geosci. 3, 398–403. https://doi.org/10.1038/ngeo866.

Gershunov, A., Cayan, D.R., Iacobellis, S.F., 2009. The great 2006 heat wave over California and Nevada: signal of an increasing trend. J. Clim. 22, 6181–6203. https://doi.org/10.1175/2009JCLI2465.1.

Gong, D.-Y., Pan, Y.-Z., Wang, J.-A., 2004. Changes in extreme daily mean temperatures in summer in eastern China during 1955–2000. Theor. Appl. Climatol. 77, 25–37. https://doi.org/10.1007/s00704-003-0019-2.

Grotjahn, R., Black, R., Leung, R., Wehner, M.F., Barlow, M., Bosilovich, M., Gershunov, A., Gutowski, W.J., Gyakum, J.R., Katz, R.W., Lee, Y.-Y., Lim, Y.-K., Prabhat, 2016. North American extreme temperature events and related large scale meteorological patterns: a review of statistical methods, dynamics, modeling, and trends. Clim. Dynam. 46, 1151–1184. https://doi.org/10.1007/s00382-015-2638-6.

Han, W., Vialard, J., McPhaden, M.J., Lee, T., Masumoto, Y., Feng, M., de Ruijter, W.P. M., 2014. Indian ocean decadal variability: a review. Bull. Am. Meteorol. Soc. 95, 1679–1703. https://doi.org/10.1175/BAMS-D-13-00028.1.

Hasanean, H.M., Almazroui, M., 2017. Teleconnections of the tropical sea surface temperatures to the surface air temperature over Saudi Arabia in summer season. Int. J. Climatol. 37, 1040–1049. https://doi.org/10.1002/joc.4758.

Hersbach, H., Coauthors, 2020. The ERA5 global reanalysis. Q. J. R. Meteorol. Soc. 146, 1999–2049. https://doi.org/10.1002/qj.3803.

Hong, C.-C., Huang, A.-Y., Hsu, H.-H., Tseng, W.-L., Lu, M.-M., Chang, C.-C., 2023. Causes of 2022 Pakistan flooding and its linkage with China and Europe heatwaves. npj Clim. Atmos. Sci. 6, 163. https://doi.org/10.1038/s41612-023-00492-2.

Horton, R.M., Mankin, J.S., Lesk, C., Coffel, E., Raymond, C., 2016. A review of recent advances in research on extreme heat events. Curr. Clim. Change Rep. 2, 242–259. https://doi.org/10.1007/s40641-016-0042-x.

Hoskins, B.J., Karoly, D.J., 1981. The steady linear response of a spherical atmosphere to thermal and orographic forcing. J. Atmos. Sci. 38, 1179–1196. https://doi.org/10.1175/1520-0469(1981)038<1179:TSLROA>2.0.CO;2.

Hu, K., Huang, G., Huang, R., 2011. The impact of tropical Indian ocean variability on summer surface air temperature in China. J. Clim. 24, 5365–5377. https://doi.org/10.1175/2011JCLI4152.1.

Hu, K., Huang, G., Qu, X., Huang, R., 2012. The impact of Indian Ocean variability on high temperature extremes across the southern Yangtze River valley in late summer. Adv. Atmos. Sci. 29, 91–100. https://doi.org/10.1007/s00376-011-0209-2.

IPCC, 2023. Weather and climate extreme events in a changing climate. In: Climate Change 2021 – the Physical Science Basis: Working Group I Contribution to the Sixth Assessment Report of the Intergovernmental Panel on Climate Change. Cambridge University Press, Cambridge, pp. 1513–1766. https://doi.org/10.1017/9781009157896.013.

Kalnay, E., Kanamitsu, M., Kistler, R., Collins, W., Deaven, D., Gandin, L., Iredell, M., Saha, S., White, G., Woollen, J., Zhu, Y., Chelliah, M., Ebisuzaki, W., Higgins, W., Janowiak, J., Mo, K.C., Ropelewski, C., Wang, J., Leetmaa, A., Reynolds, R., Jenne, R., Joseph, D., 1996. The NCEP/NCAR 40-year reanalysis Project. Bull. Am. Meteorol. Soc. 77, 437–472. https://doi.org/10.1175/1520-0477(1996)077<0437:TNYRP>2.0.CO;2.

Karoly, D.J., 1983. Rossby wave propagation in a barotropic atmosphere. Dynam. Atmos. Oceans 7, 111–125. https://doi.org/10.1016/0377-0265(83)90013-1.

Li, J., Xie, T., Tang, X., Wang, H., Sun, C., Feng, J., Zheng, F., Ding, R., 2021. Influence of the NAO on wintertime surface air temperature over East Asia: multidecadal variability and decadal prediction. Adv. Atmos. Sci. 39, 625–642. https://doi.org/10.1007/s00376-021-1075-1.

Li, J., Zheng, F., Sun, C., Feng, J., Wang, J., 2019a. Pathways of influence of the northern Hemisphere mid-high latitudes on East Asian climate: a review. Adv. Atmos. Sci. 36, 902–921. https://doi.org/10.1007/s00376-019-8236-5.

Li, L., Nathan, T.R., 1997. Effects of low-frequency tropical forcing on intraseasonal tropical–Extratropical interactions. J. Atmos. Sci. 54, 332–346. https://doi.org/10.1175/1520-0469(1997)054<0332:EOLFTF>2.0.CO;2.

Li, M., Luo, D., Yao, Y., Zhong, L., 2020a. Large-scale atmospheric circulation control of summer extreme hot events over China. Int. J. Climatol. 40, 1456–1476. https://doi.org/10.1002/joc.6279.

Li, M., Yao, Y., Simmonds, I., Luo, D., Zhong, L., Chen, X., 2020b. Collaborative impact of the NAO and atmospheric blocking on European heatwaves, with a focus on the hot

summer of 2018. Environ. Res. Lett. 15, 114003 https://doi.org/10.1088/1748-9326/aba6ad.
Liu, Y., Wang, L., Zhou, W., Chen, W., 2014. Three Eurasian teleconnection patterns: spatial structures, temporal variability, and associated winter climate anomalies. Clim. Dynam. 42, 2817–2839. https://doi.org/10.1007/s00382-014-2163-z.
Li, Y., Feng, J., Li, J., Hu, A., 2019b. Equatorial Windows and barriers for stationary Rossby wave propagation. J. Clim. 32, 6117–6135. https://doi.org/10.1175/JCLI-D-18-0722.1.
Li, Y., Li, J., 2012. Propagation of planetary waves in the horizontal non-uniform basic flow. Chin. J. Geophys. 55, 361–371. https://doi.org/10.6038/j.issn.0001-5733.2012.02.001 in Chinese.
Li, Y., Li, J., Jin, F.F., Zhao, S., 2015. Interhemispheric propagation of stationary Rossby waves in a horizontally nonuniform background flow. J. Atmos. Sci. 72, 3233–3256. https://doi.org/10.1175/JAS-D-14-0239.1.
Luo, M., Lau, N.-C., 2019. Amplifying effect of ENSO on heat waves in China. Clim. Dynam. 52, 3277–3289. https://doi.org/10.1007/s00382-018-4322-0.
Lu, R.-Y., Chen, R.-D., 2016. A review of recent studies on extreme heat in China. Atmos. Oceanogr. Sci. Libr. 9, 114–121. https://doi.org/10.1080/16742834.2016.1133071.
Matsumura, S., Yamazaki, K., 2012. Eurasian subarctic summer climate in response to anomalous snow cover. J. Clim. 25, 1305–1317. https://doi.org/10.1175/2011JCLI4116.1.
Matsumura, S., Yamazaki, K., Tokioka, T., 2010. Summertime land-atmosphere interactions in response to anomalous springtime snow cover in northern Eurasia. J. Geophys. Res. Atmos. 115 https://doi.org/10.1029/2009JD012342.
Meehl, G.A., Tebaldi, C., 2004. More intense, more frequent, and longer lasting heat waves in the 21st century. Science 305, 994–997. https://doi.org/10.1126/science.1098704.
Mora, C., Dousset, B., Caldwell, I.R., Powell, F.E., Geronimo, R.C., Bielecki, C.R., Counsell, C.W.W., Dietrich, B.S., Johnston, E.T., Louis, L.V., Lucas, M.P., McKenzie, M.M., Shea, A.G., Tseng, H., Giambelluca, T.W., Leon, L.R., Hawkins, E., Trauernicht, C., 2017. Global risk of deadly heat. Nat. Clim. Change 7, 501–506. https://doi.org/10.1038/nclimate3322.
Morice, C.P., Kennedy, J.J., Rayner, N.A., Jones, P.D., 2012. Quantifying uncertainties in global and regional temperature change using an ensemble of observational estimates: the HadCRUT4 data set. J. Geophys. Res. Atmos. 117 https://doi.org/10.1029/2011JD017187.
Parker, T.J., Berry, G.J., Reeder, M.J., Nicholls, N., 2014. Modes of climate variability and heat waves in Victoria, southeastern Australia. Geophys. Res. Lett. 41, 6926–6934. https://doi.org/10.1002/2014GL061736.
Perkins-Kirkpatrick, S.E., Gibson, P.B., 2017. Changes in regional heatwave characteristics as a function of increasing global temperature. Sci. Rep. 7, 12256 https://doi.org/10.1038/s41598-017-12520-2.
Perkins, S.E., 2015. A review on the scientific understanding of heatwaves—their measurement, driving mechanisms, and changes at the global scale. Atmos. Res. 164–165, 242–267. https://doi.org/10.1016/j.atmosres.2015.05.014.
Pfahl, S., Wernli, H., 2012. Quantifying the relevance of atmospheric blocking for co-located temperature extremes in the Northern Hemisphere on (sub-)daily time scales. Geophys. Res. Lett. 39 https://doi.org/10.1029/2012GL052261.
Rayner, N.A., Parker, D.E., Horton, E.B., Folland, C.K., Alexander, L.V., Rowell, D.P., Kent, E.C., Kaplan, A., 2003. Global analyses of sea surface temperature, sea ice, and night marine air temperature since the late nineteenth century. J. Geophys. Res. Atmos. 108 https://doi.org/10.1029/2002JD002670.
Schneidereit, A., Schubert, S., Vargin, P., Lunkeit, F., Zhu, X., Peters, D.H.W., Fraedrich, K., 2012. Large-scale flow and the long-lasting blocking high over Russia: summer 2010. Mon. Weather Rev. 140, 2967–2981. https://doi.org/10.1175/MWR-D-11-00249.1.
Sun, C., Li, J., Ding, R., Jin, Z., 2017. Cold season Africa–Asia multidecadal teleconnection pattern and its relation to the Atlantic multidecadal variability. Clim. Dynam. 48, 3903–3918. https://doi.org/10.1007/s00382-016-3309-y.
Sun, C., Li, J., Zhao, S., 2015. Remote influence of Atlantic multidecadal variability on Siberian warm season precipitation. Sci. Rep. 5, 16853 https://doi.org/10.1038/srep16853.
Sun, Y., Li, J., 2022. Synergistic effect of El Niño and the North pacific oscillation on wintertime precipitation over southeastern China and the EastEast China sea kuroshio area. Clim. Dynam. 58, 1635–1649. https://doi.org/10.1007/s00382-021-05982-8.
Su, Q., Dong, B., 2019. Recent decadal changes in heat waves over China: drivers and mechanisms. J. Clim. 32, 4215–4234. https://doi.org/10.1175/JCLI-D-18-0479.1.
Tang, Q., Zhang, X., Francis, J.A., 2014. Extreme summer weather in northern mid-latitudes linked to a vanishing cryosphere. Nat. Clim. Change 4, 45–50. https://doi.org/10.1038/nclimate2065.
Tang, X., Li, J., Zhang, Y., Li, Y., Zhao, S., 2023. Synergistic effect of El Niño and negative phase of North Atlantic oscillation on winter precipitation in the southeastern United States. J. Clim. 36, 1767–1791. https://doi.org/10.1175/JCLI-D-22-0293.1.
Wang, H., Li, J., Zheng, F., Li, F., 2023a. The synergistic effect of the summer NAO and northwest pacific SST on extreme heat events in the central–eastern China. Clim. Dynam. 61, 4283–4300. https://doi.org/10.1007/s00382-023-06807-6.
Wang, H., Li, Z., Li, J., Lin, X., Zheng, X.-T., Fan, L., Zhang, Y., 2023b. Interannual variation in the East asian summer monsoon-tropical atlantic SST relationship modulated by the interdecadal pacific oscillation. npj Clim. Atmos. Sci. 6, 169. https://doi.org/10.1038/s41612-023-00497-x.
Wang, H., Zheng, F., Diao, Y., Li, J., Sun, R., Tang, X., Sun, Y., Li, F., Zhang, Y., 2022. The synergistic effect of the preceding winter Northern Hemisphere annular mode and spring tropical North Atlantic SST on spring extreme cold events in the mid-high latitudes of East Asia. Clim. Dynam. 59, 3175–3191. https://doi.org/10.1007/s00382-022-06237-w.
Wang, J., Yan, Z., 2021. Rapid rises in the magnitude and risk of extreme regional heat wave events in China. Weather Clim. Extrem. 34, 100379 https://doi.org/10.1016/j.wace.2021.100379.
Wang, L., Wang, W.J., Wu, Z., Du, H., Shen, X., Ma, S., 2018. Spatial and temporal variations of summer hot days and heat waves and their relationships with large-scale atmospheric circulations across Northeast China. Int. J. Climatol. 38, 5633–5645. https://doi.org/10.1002/joc.5768.
Wei, J., Han, W., Wang, W., Zhang, L., Rajagopalan, B., 2023. Intensification of heatwaves in China in recent decades: roles of climate modes. npj Clim. Atmos. Sci. 6, 98. https://doi.org/10.1038/s41612-023-00428-w.
Whitham, G.B., 1960. A note on group velocity. J. Fluid Mech. 9, 347–352. S0022112060001158.
Xie, S.-P., Du, Y., Huang, G., Zheng, X.-T., Tokinaga, H., Hu, K., Liu, Q., 2010. Decadal shift in El Niño influences on indo–western pacific and East Asian climate in the 1970s. J. Clim. 23, 3352–3368. https://doi.org/10.1175/2010JCLI3429.1.
Xie, S.-P., Hu, K., Hafner, J., Tokinaga, H., Du, Y., Huang, G., Sampe, T., 2009. Indian ocean capacitor effect on indo–Western pacific climate during the summer following El Niño. J. Clim. 22, 730–747. https://doi.org/10.1175/2008JCLI2544.1.
Xie, W., Zhou, B., 2023. On the atmospheric background for the occurrence of three heat wave types in East China. Weather Clim. Extrem. 39, 100539 https://doi.org/10.1016/j.wace.2022.100539.
Xu, L., Dirmeyer, P., 2013. Snow–atmosphere coupling strength. Part II: albedo effect versus hydrological effect. J. Hydrometeorol. 14, 404–418. https://doi.org/10.1175/JHM-D-11-0103.1.
Yang, X., Zeng, G., Zhang, S., Hao, Z., Iyakaremye, V., 2021. Relationship between two types of heat waves in northern East Asia and temperature anomalies in Eastern Europe. Environ. Res. Lett. 16, 024048 https://doi.org/10.1088/1748-9326/abdc8a.
Yao, Y., Zhuo, W., Luo, D., Simmonds, I., Luo, B., Zhong, L., Huang, F., 2024. Impact of Pacific blocking on the intraseasonal winter sea ice seesaw between the Bering and Okhotsk Seas. Atmos. Res. 300, 107227 https://doi.org/10.1016/j.atmosres.2024.107227.
Zhang, L., Wang, G., Newman, M., Han, W., 2021. Interannual to decadal variability of tropical Indian ocean Sea Surface temperature: pacific influence versus local internal variability. J. Clim. 34, 2669–2684. https://doi.org/10.1175/JCLI-D-20-0807.1.
Zhang, T., Zhu, S., Song, Y., Wang, X., Chen, H., 2023. The leading modes of northern eurasian winter snowfall variability and the potential influencing factors. J. Clim. 36, 7811–7826. https://doi.org/10.1175/JCLI-D-22-0881.1.
Zhao, S., Li, J., Li, Y., 2015. Dynamics of an interhemispheric teleconnection across the critical latitude through a southerly duct during boreal winter. J. Clim. 28, 7437–7456. https://doi.org/10.1175/JCLI-D-14-00425.1.
Zhao, S., Li, J., Li, Y., Jin, F.-F., Zheng, J., 2019. Interhemispheric influence of Indo-Pacific convection oscillation on Southern Hemisphere rainfall through southward propagation of Rossby waves. Clim. Dynam. 52, 3203–3221. https://doi.org/10.1007/s00382-018-4324-y.